Revised microcalcification hypothesis for fibrous cap rupture in human coronary arteries

Adreanne Kelly-Arnold[a], Natalia Maldonado[a], Damien Laudier[a], Elena Aikawa[b], Luis Cardoso[a], and Sheldon Weinbaum[a,1]

[a]Department of Biomedical Engineering, City College of New York, New York, NY 10031; and [b]Cardiovascular Medicine, Brigham and Women's Hospital, Harvard Medical School, Boston, MA 02115

Contributed by Sheldon Weinbaum, May 13, 2013 (sent for review April 3, 2013)

Using 2.1-μm high-resolution microcomputed tomography, we have examined the spatial distribution, clustering, and shape of nearly 35,000 microcalcifications (μCalcs) ≥ 5 μm in the fibrous caps of 22 nonruptured human atherosclerotic plaques. The vast majority of these μCalcs were <15 μm and invisible at the previously used 6.7-μm resolution. A greatly simplified 3D finite element analysis has made it possible to quickly analyze which of these thousands of minute inclusions are potentially dangerous. We show that the enhancement of the local tissue stress caused by particle clustering increases rapidly for gap between particle pairs (*h*)/particle diameter (*D*) < 0.4 if particles are oriented along the tensile axis of the cap. Of the thousands of μCalcs observed, there were 193 particle pairs with $h/D \leq 2$ (tissue stress factor > 2), but only 3 of these pairs had $h/D \leq 0.4$, where the local tissue stress could increase a factor > 5. Using nondecalcified histology, we also show that nearly all caps have μCalcs between 0.5 and 5 μm and that the μCalcs ≥ 5 μm observed in high-resolution microcomputed tomography are agglomerations of smaller calcified matrix vesicles. μCalcs < 5 μm are predicted to be not harmful, because the tiny voids associated with these very small particles will not explosively grow under tensile forces because of their large surface energy. These observations strongly support the hypothesis that nearly all fibrous caps have μCalcs, but only a small subset has the potential for rupture.

finite element analysis of fibrous caps | microcomputed tomography imaging of microcalcifications | vulnerable plaque | clustered microcalcifications

Fibrous cap rupture and the ensuing thrombus formation account for more than 50% of all cardiovascular deaths in the United States. Before the study by Vengrenyuk et al. (1), nearly all studies of human coronary artery calcification had focused on macrocalcifications that were visible using in vivo imaging techniques (2). Although coronary calcification is clinically related to poor prognosis and used as a marker for the advancement of the disease (3), it has not been successfully correlated with cap rupture (2, 4–6). The work by Vengrenyuk et al. (1) was a major departure from this approach, in that it attributed cap rupture to cellular-level microcalcifications (μCalcs) in the cap proper as opposed to macrocalcifications (calcifications > 100 μm), which finite element analysis (FEA) (4) predicted reduced peak circumferential stress (PCS). In contrast, the models in refs. 1, 7, and 8 predicted that μCalcs acted as local tissue stress concentrators in the fibrous cap proper, causing a nearly twofold increase in local tissue stress for spherical μCalcs independent of their size and location in the cap.

Cap rupture is frequently viewed as an inflammatory response affecting material properties, and thus, it is especially puzzling that 37% of tears occur in the center of the cap (9, 10), when macrophage infiltration is largely observed near the shoulders, and that the densest collage structure is typically at the cap center (9). Vengrenyuk et al. (1) proposed that the doubling of tissue stress caused by the presence of a μCalc could explain this paradoxical observation. The existence of such μCalcs in the fibrous cap was also shown for a single vulnerable lesion using 6.7-μm high-resolution microcomputed tomography scanning (HR-μCT), where three nearly spherical inclusions of ~20-μm diameter were observed. Vengrenyuk et al. (1) suggested that the μCalcs were calcified macrophages or smooth muscle cells and that the triggering event was an interfacial debonding caused by the large mismatch in material properties between the μCalc and the surrounding tissue. Vengrenyuk et al. (1) believed that cap rupture was relatively rare, because only one of five fibrous caps that they examined contained such inclusions. In contrast, numerous μCalcs were observed in the necrotic core, where they were treated as floating debris and thus, not biomechanically dangerous.

The much more comprehensive recent study by Maldonado et al. (10), where 62 nonruptured fibrous cap atheromas were examined in 92 arteries of the three major coronary arteries (also at 6.7-μm resolution HR-μCT), has suggested a greatly revised view of the role of μCalcs in fibrous cap rupture. These 92 arteries had, on average, 4,160 μCalcs; 85% of μCalcs were <50 μm, with the vast majority residing in lipid pools. Only 0.2% of these μCalcs (81 total) were in the fibrous cap proper, where they could act as tissue stress concentrators. Strikingly, all 81 of the imbedded μCalcs were confined to just 9 (15%) of 62 fibroatheromas, and their average size was 28 ± 13 μm. The remaining 53 nonruptured atheromas had no visible μCalcs at 6.7-μm resolution HR-μCT, the thinnest of these caps being 66 μm (close to the <65-μm minimum thickness criterion for rupture proposed in ref. 11).

3D FEA was performed on all 81 of the μCalcs described above and the thinnest cap (66-μm cap) without visible μCalcs. The highest predicted tissue stress for all 81 μCalcs was 275 kPa, confirming the 300-kPa threshold for rupture proposed in ref. 12. More significantly, the 66-μm cap had a PCS of only 107 kPa, far below the rupture threshold. FEA showed that this cap would have to thin to ~30 μm to achieve the 300-kPa rupture threshold; however, there was not a single nonruptured cap between 30- and 66-μm thickness among these 53 nonruptured lesions. Maldonado et al. (10) conjectured that these paradoxical observations could be explained if all caps between 30 and 66 μm had ruptured—not because of their thickness but because of the presence of μCalcs that were just not visible using 6.7-μm resolution HR-μCT. 3D FEA also showed that local stress concentrations could be increased not two- but fivefold in the tissue space between μCalcs when they were in close proximity.

The present paper has taken these results and conjectures into a different realm. The same arterial specimens examined in the study by Maldonado et al. (10) have been reexamined at 2.1-μm resolution HR-μCT, a resolution capable of detecting inclusions as small as ~5 μm. Instead of 81 μCalcs in nine caps, one is now able to resolve nearly 35,000 μCalcs in 22 caps (one-third of all atheromas), strongly supporting the conjecture in the study by Maldonado et al. (10) that the vast majority of μCalcs in caps was not visible at 6.7-μm resolution. Such a large number of μCalcs required a new simplifying analysis, in which one could quickly

Author contributions: L.C. and S.W. designed research; A.K.-A., N.M., D.L., E.A., L.C., and S.W. performed research; N.M., D.L., and E.A. contributed new reagents/analytic tools; A.K.-A., N.M., L.C., and S.W. analyzed data; and A.K.-A., N.M., L.C., and S.W. wrote the paper.

The authors declare no conflict of interest.

Freely available online through the PNAS open access option.

[1]To whom correspondence should be addressed. E-mail: weinbaum@ccny.cuny.edu.

This article contains supporting information online at www.pnas.org/lookup/suppl/doi:10.1073/pnas.1308814110/-/DCSupplemental.

identify and theoretically analyze the local tissue stress in potentially dangerous μCalc clusters and calcification geometries. In addition, histological methods that do not require decalcification for sectioning clearly showed μCalcs between 0.5 and 5 μm in nearly all of the remaining lesions. These studies provide the necessary resolution to reveal the fine structure of the smallest μCalcs visible in 2.1-μm resolution HR-μCT and suggest the connecting link between the agglomeration of calcified matrix vesicles (13–15) and μCalcs currently visible in HR-μCT. This finding is supported by the in vivo molecular imaging studies of Aikawa et al. (14, 16), which link μCalcs and plaque rupture in inflamed mouse and human atheromas.

In view of the huge number of μCalcs now observed in the fibrous caps proper, one is confronted with a fundamental paradox: why did the 22 caps, which had, on average, 1,564 μCalcs/cap > 5 μm, not rupture? We show that there are two basic reasons for this failure to rupture. First, the amplification of the local tissue stress depends primarily on a single parameter: the gap between the μCalcs (h)/their diameter (D). 3D FEA shows that large amplifications (>5) in tissue stress only occur when $h/D < 0.4$ and the particles are oriented along the tensile axis of the cap. Of nearly 35,000 μCalcs observed, there were only 193 particle pairs with $h/D < 2$; only three of these pairs had $h/D < 0.4$. Second, as recently shown in the study by Maldonado et al. (17), using cavitation theory for the explosive growth of small voids in hyperelastic materials (18), the actual triggering event for cap rupture is the explosive growth of small voids in the gap between closely spaced μCalcs (cavitation) and not interfacial debonding, which was proposed in ref. 1. Cavitation in a hyperelastic solid should not be confused with a well-known phenomenon in fluid mechanics, where small bubbles grow when their vapor pressure exceeds the local fluid pressure of the surrounding fluid. In a tissue that contains cells, collagen, and elastin, the likely origin of these voids is dissolved gases, which come out of solution when the local pressure is reduced because of tension. However, voids that are very small (<500 nm) have a surface energy that can far exceed the energy needed for cavitation, preventing their explosive growth.

These new results have led to a major modification of the original microcalcification hypothesis advanced in ref. 1, namely that μCalcs in fibrous caps are not rare but numerous, that they are not calcified macrophages or smooth muscle cells but an agglomeration of cell-derived calcified matrix vesicles, and that there is a minimum critical size of ~5 μm for them to be potentially dangerous.

Results

Specimens and Scanning Procedure. Sixty-six human coronary fibroatheromas, defined as thickened vessel walls with visible lipid pool and necrotic core, were detected by 2.1-μm HR-μCT scanning in 92 human coronary arteries harvested from 32 formaldehyde-fixed whole hearts obtained from the National Disease Research Interchange. Four vessels were excluded, because they contained stents. Sixty-six fibroatheromas are four more than the sixty-two fibroatheromas reported in ref. 10, because at 2.1-μm resolution, there was a significantly improved definition of lipid pools and necrotic cores (Fig. 1 and *SI Text*).

μCalc Size Distribution, Cap Thickness, and Location. The automated 3D analysis of the HR-μCT images of the fibrous caps using CTAn software (v11.0; SkyScan) revealed thousands of μCalcs of different sizes, with equivalent spherical diameters ranging from 5 to 50 μm, in 22 of 66 caps analyzed. These 22 fibrous caps, where particles > 5-μm diameter were visible at 2.1-μm resolution, contained, in total, 34,408 μCalcs and on average, 1,564 ± 2,506 μCalcs/cap. A summary of the size distribution and minimum cap thickness for all 22 caps is shown in Table 1. Also shown for comparison is the size distribution for 81 μCalcs observed in ref. 10 (Table 2). One notes that 79.6% of the μCalcs were between 5- and 15-μm D based on their measured volume, $V = \pi D^3/6$, 17.7% of the μCalcs were between 15- and 30-μm D, and 2.7% of the μCalcs were between 30- and 50-μm D. Minimum cap thicknesses varied between 35 and 285 μm.

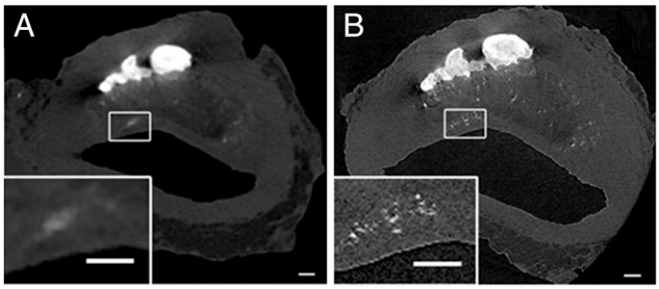

Fig. 1. HR-μCT images of human coronary atheroma with μCalcs embedded in the fibrous cap proper. *A* shows images scanned at 6.7-μm resolution. *B* was scanned at 2.1-μm resolution. Multiple μCalcs in the cap are visible in *B Inset* that were previously undetected in *A*. *A Inset* and *B Inset* show the difference between what appears to be a single μCalc at 6.7 μm and μCalc clusters when viewed at 2.1-μm resolution. (Scale bar: 100 μm.)

Clearly, few, if any, μCalcs < 15-μm diameter were observed at 6.7-μm resolution, where the mean size was reported as 28 ± 13 μm. However, there are large discrepancies in the size distribution for μCalcs in the 15- to 30-μm and 30- to 50-μm size ranges for the nine caps with μCalcs analyzed in ref. 10. These discrepancies have two origins. First, there is a much sharper definition of the boundaries of the lipid pool or necrotic core in the present study compared with the study by Maldonado et al. (10), as clearly shown by comparing the image in Fig. 1*A* with the image in Fig. 1*B*. Many of the μCalcs reside near the lipid pool boundary, especially its top surface, and these μCalcs were treated as being in the lipid pool in our earlier study. Second, most of the μCalcs in the cap in Fig. 1*B* were invisible in Fig. 1*A*, where they had a collective clouded light gray appearance. μCalcs at 6.7-μm resolution, which had the appearance of a single larger μCalc, were actually a cluster of smaller μCalcs. Thus, the percentage distribution of μCalcs in the 30- to 50-μm group is much smaller than in the 15- to 30-μm group. However, the most important observation in Table 1 is that, except for specimen 11, there were hundreds to thousands of μCalcs ≥ 5 μm in 22 caps in Table 1. This finding is far beyond what one could analyze using finite element approaches, especially given the spatial heterogeneity of their distribution. The 44 caps with no distinct visible μCalcs, even at 2.1-μm resolution, will be described later.

Because 37% of cap ruptures occur in the central region of the cap (8, 9), we wished to see if this location correlates with the distribution of μCalcs in the cap. Specimen 8 was selected for this purpose, because its cap was well-defined and contained a large number of μCalcs. The central region was defined as the inner 50% of the cap, and the shoulders were defined as the outer 25% of the cap length on each end. We observed that 506 or 33% of 1,542 μCalcs were positioned in the central region. These results support the observations in ref. 10, where 42% of 81 μCalcs examined resided in the center of the cap.

We also examined whether the presence of fibrous caps with μCalcs > 5 μm coincide with locations of stenosis, because more than one-half of vulnerable lesions exhibit relatively minor stenosis (19). The degree of stenosis varied between 12% and 60%, and only 30% of atheromas showed clusters of μCalcs in the vicinity of maximum stenosis.

μCalc Spacing and Orientation. The volume V and surface S measured for each particle using CTAn were used to calculate its approximate aspect ratio major axis (l)/minor axis (r) if the particle was treated as an ellipsoid of revolution (*SI Text*). To calculate the distance between particles, $h = d_{cen} - r_a - r_b$, where d_{cen} is the distance between the centroids of particles a and b based on their effective diameter.

Although there can be several thousand μCalcs > 5 μm in a single cap, a very unusual simplification was first observed in ref. 17. Until 2005, all FEA of tissue stresses in coronary arteries was based on 2D cross-sections of arteries. Using this approach,

Table 1. Cap thickness and μCalc size distribution in fibrous cap (2.1-μm resolution)

				Size distribution (μm) of μCalcs in caps					
				$5 < D < 15$		$15 < D < 30$		$30 < D < 50$	
Sp. no.	Stn (%)	MCT (μm)	No. of μCalcs	No. of μCalcs	%	No. of μCalcs	%	No. of μCalcs	%
1	40	254	48	45	94	2	4	1	2
2	56	149	149	113	76	31	21	5	3
3	44	286	1,827	1,371	75	394	22	62	3
4	13	206	795	554	70	200	25	41	5
5	44	56	3,324	2,550	77	636	19	138	4
6	34*	126	474	379	80	78	16	17	4
7	39*	98	565	319	56	199	35	47	8
8	45	111	1,542	1,281	83	231	15	30	2
9	37	58	492	465	95	27	5	0	0
10	56	228	1,244	800	64	371	30	73	6
11	23	182	35	26	74	3	9	6	17
12	53*	98	1,646	1,516	92	121	7	9	1
13	35	143	4,016	2,984	74	901	22	131	3
14	34	70	194	177	91	17	9	0	0
15	41	75	598	470	79	128	21	0	0
16	31	110	1,368	1,094	80	263	19	11	1
17	50*	70	1,975	1,761	89	187	9	27	1
18	32*	77	12,088	9,931	82	1,918	16	239	2
19	28*	86	532	389	73	121	23	22	4
20	12	NM	638	449	70	150	24	39	6
21	34	80	248	217	88	28	11	3	1
22	60	35	610	498	82	101	17	11	2
Total			34408	27,389	79.3	6,107	17.2	912	3.5
Mean	38	123.7	1,564.0	1,245.0		277.6		41.5	
SD	14	69.8	2,565.2	2,097.3		426.3		58.9	

D, equivalent spherical diameter; MCT, minimum cap thickness; No. of μCalcs, number of microcalcifications; NM, not measurable; Sp. no., specimen number; Stn, percentage of stenosis.
*μCalcs located near the maximum stenosis site.

Maldonado et al. (17) calculated the stress concentration factor for two circular inclusions in a uniform thickness cap when the inclusions were aligned along the tensile axis of the cap, treating the inclusions as circular cylinders. The purpose was to try and explain how one could obtain stress concentration factors that were as great as a factor of five for the 81 μCalcs observed in arteries 1–9 in Table 2. It was evident that μCalcs in close proximity, $h/D < 0.4$, had an effect that was not just additive but increased exponentially with decreasing h/D. For two circular cylinders, the increase in stress seemed to depend primarily on a single-parameter h/D. The calculation just described has now been performed for two spherical inclusions along the tensile axis of the cap using a fully 3D FEA. This result is reported in Fig. 2*A* along with the corresponding 2D solutions obtained in ref. 17.

Fig. 2*A* shows that the calculated stress concentration factor is a factor of two for $h/D > 1$, which is nearly the same as for an isolated spherical inclusion, but it increases exponentially for $h/D < 0.4$, where the local stress could increase more than 500%. The results are independent of the size of the particle, its position within the cap, and the cap thickness, which was 140 μm for the results shown. A substantial difference develops between the 2D and 3D results for $h/D < 0.5$. When two spheres are put in tension, one creates a strain in the region between the spheres, which grows rapidly as the gap between them decreases. The amount of tissue to absorb this strain energy is much smaller for two spheres than two cylinders, resulting in a significantly larger increase in the stress concentration factor for the 3D geometry. If the tensile force was applied transverse to the particle axis, one would obtain results close to a factor of two, the same as for an isolated particle. A comparison of the tissue stresses in the gap between the particles for the two cases with the same h/D and cap thickness is shown in Fig. 2*B*. One notices that a large strain (45%) develops in the gap between the μCalcs when they are oriented along the tensile axis, whereas the gap narrows by 30% when tensile forces act transverse to the μCalc axis.

Fig. 2*A* provides an enormous simplification. One could not possibly perform an FEA on a cap with several thousand μCalcs > 5 μm. However, one does not have to perform this analysis. One only needs to perform an FEA on the basic vessel geometry without μCalcs to determine the background stress distribution and then calculate the stress amplification factor for the most closely spaced μCalcs. To illustrate the importance of

Table 2. μCalc size distribution in fibrous cap (6.7-μm resolution)

		Size distribution (μm) of μCalcs in caps					
			$15 < D < 30$		$30 < D < 50$		
Sp. no.	No. of μCalcs	$5 < D < 15$	No. of μCalcs	%	No. of μCalcs	%
1	5	n/a	3	60	2	40
2	5	n/a	3	60	2	40
3	16	n/a	9	56	7	44
4	11	n/a	1	9	10	91
5	15	n/a	9	60	6	40
6	9	n/a	6	67	3	33
7	11	n/a	3	27	8	73
8	5	n/a	2	40	3	60
9	4	n/a	2	50	2	50
Total	81		38	47	43	53
Mean	9.00		4.22		4.78	
SD	4.56		3.03		3.03	

D, equivalent spherical diameter; No. of μCalcs, number of microcalcifications; n/a, not applicable; Sp. no., specimen number.

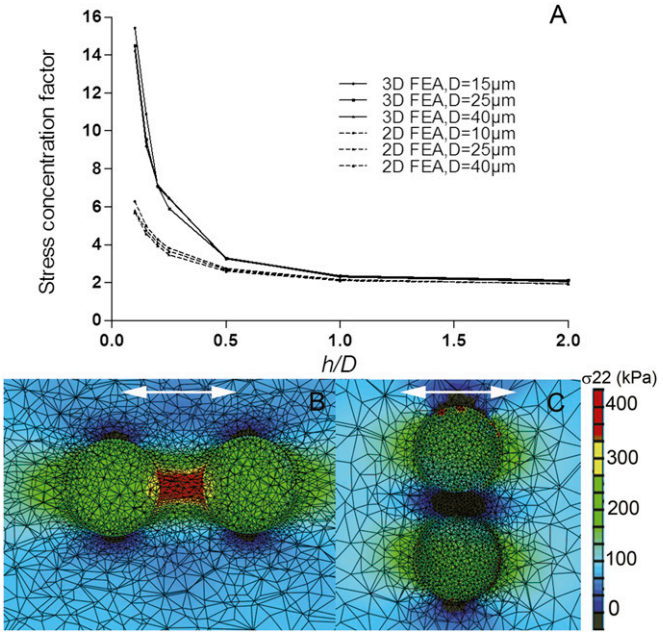

Fig. 2. (*A*) 3D FEA results of stress concentration factor calculated for the area between two particles located along the tensile axis in a fibrous cap. Stress concentration factor rises exponentially when the distance between the two spherical μCalcs decreases. Results are compared with previous 2D FEA reported in the work by Maldonado et al. (10). *B* and *C* show FEA results for particles with initial $h/D = 0.4$ oriented along and tensile the transverse axis, respectively.

this simplification, nearly 35,000 μCalcs > 5 μm were analyzed in 22 caps described in Table 1. Using the CTAn analysis software, we were able to, in 1 h, identify the locations of all 35,000 μCalcs and the position of their closest neighbors. The availability of much higher-resolution HR-μCT images enabled us to quickly estimate the h between particles and their D. The remarkable result is that there were only 193 pairs of μCalcs in all 22 caps where $h/D < 2$ and that there were only 3 pairs where h/D was < 0.4, where one would anticipate a large increase in the stress concentration factor. The distribution of 193 μCalc pairs with $h/D < 2$ is shown in Fig. 3. The three cases with $h/D \leq 0.4$ are described in more detail in *Finite Element Models* using a 3D FEA. For $h/D > 2$, the inclusions can be treated as isolated particles; there is little interaction between them, and their stress concentration factor is roughly two, unless they are elongated. Although the particles can take complex geometries, this complexity is not difficult to handle, which is shown in *Nonspherical μCalcs*.

Finite Element Models. Closer examination of Table 1 reveals that there are at least six caps that require additional analysis to understand why they did not rupture. These specimens are specimens 5, 7, 15, 17, 19, and 22. These six patient-specific atheromas had between 532 and 3,324 μCalcs visible in their fibrous caps. All six specimens had at least one region with cap thickness < 100 μm. Specimen 22 corresponds to the thinnest cap of 66 analyzed caps with a minimum cap thickness of 35 μm. Although this cap had 610 μCalcs ≥ 5 μm, none were located in the region of minimum thickness to further increase vulnerability to rupture. Specimens 15 and 19 were selected, because they correspond to thin caps where μCalcs were detected near the region of minimum cap thickness. Specimens 5, 7, and 17 were selected from the results in Figs. 2 and 3. These three specimens correspond to the three lowest values of h/D in Fig. 3, where $h/D < 0.4$ and the stress concentration factor is > 5. A seventh fibroatheroma was also analyzed. This specimen was shown in figure 8 in ref. 10, where a 20-μm μCalc was observed imbedded in the tip of a ruptured cap at the precise location of the tear. In this case, the cap was reconstructed, preserving the volume of soft tissue in the cap that is pressurized to 110 mmHg, and FEA was applied to determine the PCS at the rupture site with and without the culprit μCalc. This reconstruction is described in Fig. S1. In HR-μCT grayscale imaging, it is very difficult to capture a rupture, because the thrombus cannot be distinguished from the surrounding soft tissue unless the thrombus detaches and washes downstream, leaving the imbedded culprit μCalc behind.

To construct patient-specific HR-μCT–based FEA models, HR-μCT images of the seven atheromas described above were imported into Mimics software (v.13.0; Materialize), where lipid calcification and fibrous cap were segmented based on density-calibrated images. A linear tetrahedral mesh representing the geometry was created, and material properties were then assigned using an incompressible neo-Hookean isotropic model. The value of Young's modulus of the lipid core was prescribed to be $E_{lipid} = 5$ kPa, the soft tissue was $E_t =$ 500 kPa, and $E_{calc} = 10$ GPa (20, 21). At the lumen of the artery, a pressure of 110 mmHg (14.6 kPa) was applied. A 3D model was created using ABAQUS (v.6.12; Dassault). The background stress distribution in the fibrous cap was calculated by replacing the μCalcs with soft tissue, and the circumferential stress at that location was considered as the background stress. To calculate the PCS, including the effect of μCalcs, the stress concentration factor, shown in Fig. 2*A*, was applied at the location of the minimum h/D (specimens 5, 7, and 17) or minimum cap thickness (specimens 15 and 19). This approach allowed PCS to be calculated without individually modeling thousands of μCalcs using FEA, dramatically reducing the computational cost. These results are summarized in Table 3.

For specimen 22, the thinnest cap, PCS of 313 kPa, did occur in a region of minimum thickness where there were no μCalcs. The minimum h/D of 1.3 caused a twofold increase in local tissue stress, but this stress was in a location where the cap was thicker and thus, did not affect PCS. Specimens 15 and 19 did have μCalcs in the region of minimum cap thickness, and the values of h/D (1.0 and 0.6) caused a 2.3 and 2.7 amplification of the background tissue stress, respectively. However, this PCS was not nearly sufficient to raise the tissue to the 300-kPa threshold, because the background stress was low in the region of minimum cap thickness. Thus, cap thickness alone does not determine the background stress, because factors, like necrotic core size and thickness, directly modify it (20). Specimens 5 and 7, which had stress amplification factors of 7.0 and 5.0, respectively, similarly were not close to the rupture threshold, because they were in regions where the background stress was low. The most intriguing of the six atheromas was specimen 17, which had an h/D of 0.28 and a stress concentration factor of 5.3, which would have led to an estimated PCS of 471 kPa, clearly sufficient to cause rupture. However, when this case was more closely examined, it was observed that the μCalcs were oriented roughly 75° to the tensile axis and that the stress concentration factor was closer to 2.0, the result for a transverse orientation shown in Fig. 2*C*.

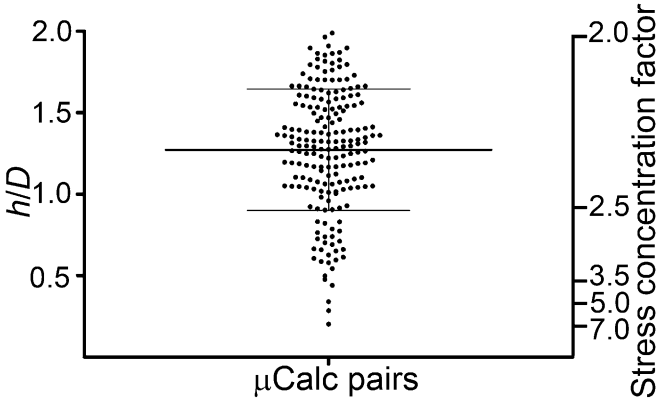

Fig. 3. Ratio h/D for 193 pairs of μCalcs embedded in fibrous caps where $h/D < 2$ and the corresponding stress concentration factor when embedded in a fibrous cap along the tensile axis. Lines indicate mean ± SD.

Table 3. Results for HR-μCT–based FEA of PCS in human fibrous caps

Sp. no.	MCT (μm)	No. of μCalcs	μCalcs at MCT	BG stress (kPa)	Minimum *h/D*	SCF	PCS (kPa)
5	57	4,155	No	37	0.34	5.0	185.0
7	98	630	No	29	0.2	7.0	203.0
15	75	762	Yes	85	1.0	2.3	195.5
17	70	2,834	No	89	0.28	5.3	471.7
19	86	641	Yes	35	0.6	2.7	94.5
22	35	742	No	313	1.3	1.0	313.0

BG stress, background stress; MCT, minimum cap thickness; μCalcs at MCT, μCalcs located in region of MCT; Minimum *h/D*, minimum separation to equivalent spherical diameter ratio; No. of μCalcs, number of microcalcifications; PCS, peak circumferential stress; SCF, stress concentration factor; Sp. no., specimen number.

Finally, for our reconstructed ruptured plaque from the study by Maldonado et al. (10) (Fig. S1*C*), our 3D FEA showed that, in the absence of the μCalc, PCS would have been 210 kPa, which is significantly less than the 300-kPa threshold for rupture. However, when considering the presence of the μCalc embedded in the fibrous cap at the rupture site, the PCS rises to 396 kPa (Fig. S1*D*), which could easily explain the rupture.

Nonspherical μCalcs. The greatly increased resolution of the HR-μCT images allowed us to not only obtain a much better estimation of the number of μCalcs present in the fibrous cap proper but also, estimate their shape. Using the formulas for the sphericity and volume of each particle described in *SI Text*, one can calculate the aspect ratio of an equivalent prolate spheroid with the same volume and surface area. In Fig. S2, we have plotted the percentage of μCalcs as a function of their aspect ratio l/D using these relations for an equivalent prolate spheroid. Approximately 35% of μCalcs have an $l/D < 2$; $2 < l/D < 3$ for 35% of μCalcs, and $3 < l/D < 4$ for 15% of μCalcs, leaving $4 < l/D < 8$ for roughly 15% of μCalcs. Vengrenyuk et al. (7) have shown that, whereas a near-spherical μCalc would cause a twofold increase in PCS, a prolate spheroid with an aspect ratio $l/D > 2$ could cause more than a fourfold increased stress in a localized region near its ends.

A much better estimation of the shape of μCalcs along with an insight into the origin of the μCalcs can be obtained from transmission electron microscopy (TEM) images and nondecalcified histology. Fig. 4 *A* and *B* show μCalcs embedded in a mouse atheroma and human fibrous cap, respectively. Both μCalcs have a shape consistent with the agglomeration of several enlarged cell-derived matrix vesicles, where the region beneath the membrane has started calcifying after coalescence. As observed in Fig. 4 *A* and *B*, an elongated μCalc is an agglomeration of smaller calcified particles, which individually, have the shape of ellipsoids of revolution.

The TEM-based FEA calculated stress concentration factor at the poles of the particle in Fig. 4*A* is shown in Fig. 4*C*, indicating that the presence of this elongated particle would increase local stress 3.7 and 4.2 times at its ends instead of the twofold increase calculated for its volume-equivalent sphere. For our histologically constructed μCalc in Fig. 4*B*, the increase in stress at its ends is 5.0 and 6.4 (Fig. 4*D*). Our FEA indicates that two key shape parameters determine PCS at the poles of a μCalc: (*i*) length along the tensile axis and (*ii*) curvature of the μCalc complex at its poles.

Discussion

The initial formulation of the μCalc plaque rupture hypothesis (1) was based on an idealized model for a single spherical inclusion and the observation of three cellular-level μCalcs in the fibrous cap proper of a single fibroatheroma at 6.7-μm resolution HR-μCT. It is not unexpected that, with the current observation of nearly 35,000 μCalcs at significantly higher resolution and nondecalcified histology to see even smaller μCalcs, this original formulation requires major modification. Vengrenyuk et al. (1) suggested that the μCalcs were a relatively rare occurrence, that μCalcs derived from apoptotic macrophages trapped in the cap while moving to the necrotic core, and that rupture was caused by interfacial debonding at the μCalc interface. With evolved understanding of the biology of microcalcification and improved imaging resolution, our recent studies (10, 17) can be viewed as a critical transition, where each of these hypotheses is initially questioned.

The observation of nearly 35,000 μCalcs > 5 μm in 22 of 66 human fibrous caps provides indisputable evidence that μCalcs of these dimensions are, indeed, numerous and that the 81 μCalcs observed in ref. 10 in 15% of the caps at 6.7-μm resolution were a gross underestimation. Table 1 shows that the size of 80% of the μCalcs was between 5 and 15 μm, and thus, they were not visible at 6.7-μm resolution. Also, many μCalcs believed to be a single particle at 6.7-μm resolution were actually clusters of smaller μCalcs (Fig. S3). Similarly, particles between 30 and 50 μm seen at 6.7-μm resolution were clusters of 15- to 30-μm particles, causing a large percentage difference in the particle size distribution at 2.1- and 6.7-μm resolutions for the larger μCalcs. Not a single μCalc > 50 μm was seen in the fibrous cap proper, the current threshold for in vivo imaging. Additionally, histology images reveal the presence of μCalcs between 0.5 and 5.0 μm in the remaining 44 fibrous caps (Fig. S3*C*), confirming recent reports of μCalcs < 1 μm in fibrous caps in the works by New and Aikawa (22) and Roijers et al. (23).

With so many μCalcs, why are there not more ruptures? FEA and our criterion for identifying which of the thousands of μCalcs are potentially dangerous provide the key insights into this critical question. The data in Figs. 2 and 3 and Table 3 are crucial to understanding why these caps did not rupture. First, the μCalcs have to be in a local region where the background stress is already elevated, typically a region where the cap is thin. The minimum thickness of specimen 22 was only 35 μm, but no μCalcs were observed in this region where the PCS was 313 kPa, very close to the 300-kPa minimum threshold for rupture (12). Contrary to widely held beliefs, cap thickness by itself is not the only criterion. Even for a thin cap, a single μCalc at the right location would greatly increase rupture risk. Second, clusters of

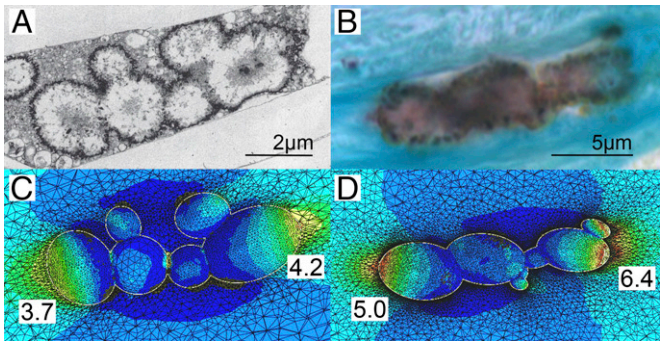

Fig. 4. TEM and histology-based FEA. (*A*) TEM image of aggregated calcifying matrix vesicles forming μCalcs in a mouse atheroma. (*B*) Image of a μCalc embedded in a human fibrous cap, obtained from nondecalcified histology, and stained with von Kossa. (*C* and *D*) Stress distribution at the interface of the μCalcs in *A* and *B*, respectively, assuming that they are embedded in fibrous caps under tension. Numbers show calculated stress concentration factors at the poles.

particles in close proximity, $h/D < 0.4$, produce a stress concentration factor that is much greater than a single μCalc provided that the particles are aligned with the tensile axis. This concept is supported by the study by Gent and Park (18) that shows that a tiny void has to preexist in the region of the stress concentration. This possibility is not likely for a single particle, because the region of increased stress is confined to small regions in the immediate vicinity of the tensile poles. In marked contrast, the entire region between two μCalcs in close proximity will be exposed to this high stress (Fig. 2*B*). Third, we observed that there were only three particle pairs with $h/D \leq 0.4$ among all 22 caps with μCalcs > 5 μm that had not ruptured. In all three specimens 5, 7, and 17 in Table 3, FEA showed that the 300-kPa threshold for rupture had not been exceeded. In a dataset of 35,000 μCalcs, this finding is remarkable. We cannot confirm it in the present study, but a plausible conclusion is that the failure to find other particle pairs with $h/D \leq 0.4$ meant that these caps had ruptured.

Our nondecalcified histology of human fibrous caps and EM of μCalcs in the cap of an apolipoprotein E knockout (APO-$E^{-/-}$) mouse in Fig. 4 strongly suggest that μCalcs are derived from matrix vesicles, which could be formed from smooth muscle cell or macrophage membrane blebs (24). These membrane-bound bodies, which are initially 100–300 nm, can merge to form larger vesicles or μCalcs (13–15). Bobryshev et al. (13) estimated that ∼1% of matrix vesicles calcify in their initial state. Fig. 4 suggests that these small vesicles first fuse to form larger vesicular bodies, typically 1- to 2-μm diameter, that then calcify and agglomerate. Calcification appears to start at the membrane and then may proceed inward. Even at 2.1-μm resolution HR-μCT, it is difficult to image the shape of small μCalcs. However, volume and sphericity measurements in Fig. S2 indicate that 65% of the μCalcs have an aspect ratio > 2.

Although μCalcs < 5 μm cannot be seen at 2.1-μm resolution HR-μCT, they are clearly visible in nondecalcified histology using either Alizarin Red S or von Kossa stain. These very small μCalcs do not initiate plaque rupture as explained in detail in ref. 17. Originally, Vengrenyuk et al. (1) proposed that the triggering event for rupture was an interfacial debonding that started at the poles of the inclusion. The theory for hyperelastic materials developed in ref. 18 and applied in ref. 17 for spherical μCalcs shows that, for debonding to occur, the strain energy stored in the tissue at the poles of a μCalc in tension must exceed the bonding energy at the surface of the particle. This stored energy increases with the size of the particle and for representative adhesion strengths debonding theory (18), predicts that the particle must exceed 65-μm diameter. No μCalcs of this dimension have been observed among 35,000 μCalcs in this study. A more plausible possibility is cavitation, the explosive growth of a small void when the tissue stress exceeds ∼5/6E, where E is the Young's modulus of the material. Because the measured value of E is typically 500 kPa, this threshold for cavitation falls precisely in the range 300–545 kPa that has been widely used for cap rupture. Initial voids seldom exceed about 1/10th of the particle radius (18). Thus, a 5-μm inclusion would have an initial void < 500 nm. The calculations in ref. 17 show that the surface energy to expand such a tiny void would far exceed 5E/6 and that cavitation would not occur.

Unfortunately, the distribution of the μCalcs is heterogeneous, and thus, one cannot apply homogenization theory, such as in the work by Wenk et al. (25), for predicting local tissue stress. However, there is a single parameter, h/D, that seems to predict the local amplification factor for tissue stress when neighboring μCalcs are aligned along their tensile axis, the worst case scenario. This parameter enables one to quickly single out which μCalcs are the most dangerous in a cap with hundreds to thousands of μCalcs < 5 μm without doing very costly, if not insurmountable, FEA. The principle limitation of the present study is that it is based nearly exclusively on the analysis of caps that have not ruptured and the interpretation of now extensive data to explain why rupture has not occurred. Although they have not been treated in this paper, other biological processes can alter the Young's modulus E of the tissue. Because the requirement for cavitation is that the local tissue stress exceed 5E/6, processes such as enzymatic degradation and erosion, which decrease E, will lower the threshold stress for cavitation, whereas matrix synthesis will increase E and increase this threshold. Another important factor, which is described in the work by Ohayon et al. (26), is the influence of residual stresses. These stresses typically put the inner wall of the artery in compression and can reduce the local background stress by as much as a factor of two, significantly reducing the PCS and hence, the likelihood of cavitation.

ACKNOWLEDGMENTS. This research has been supported by National Institutes of Health Grant R01 HL114805-01 (to E.A.), National Science Foundation Major Research Instrumentation (MRI) Grants 0723027 (to L.C.) and 1229449 (to L.C.), and National Institutes of Health American Recovery and Reinvestment Act (ARRA) Grants RCI HL101151 (to S.W.) and AG034198.

1. Vengrenyuk Y, et al. (2006) A hypothesis for vulnerable plaque rupture due to stress-induced debonding around cellular microcalcifications in thin fibrous caps. *Proc Natl Acad Sci USA* 103(40):14678–14683.
2. Burke AP, Kolodgie FD, Farb A, Virmani R (2007) Pathogenesis and significance of calcification in coronary aterosclerosis. *The Vulnerable Atherosclerotic Plaque: Strategies for Diagnosis and Management*, eds Virmani R, Narula J, Leon M, Willerson JT (Blackwell, Oxford), pp 77–94.
3. McCollough CH, et al. (2007) Coronary artery calcium: A multi-institutional, multimanufacturer international standard for quantification at cardiac CT. *Radiology* 243(2):527–538.
4. Huang H, et al. (2001) The impact of calcification on the biomechanical stability of atherosclerotic plaques. *Circulation* 103(8):1051–1056.
5. Kume T, et al. (2011) Assessment of the coronary calcification by optical coherence tomography. *EuroIntervention* 6(6):768–772.
6. Thilo C, et al. (2010) Correlation of regional distribution and morphological pattern of calcification at CT coronary artery calcium scoring with non-calcified plaque formation and stenosis. *Eur Radiol* 20(4):855–861.
7. Vengrenyuk Y, Cardoso L, Weinbaum S (2008) Micro-CT based analysis of a new paradigm for vulnerable plaque rupture: Cellular microcalcifications in fibrous caps. *Mol Cell Biomech* 5(1):37–47.
8. Maehara A, et al. (2002) Morphologic and angiographic features of coronary plaque rupture detected by intravascular ultrasound. *J Am Coll Cardiol* 40(5):904–910.
9. Richardson PD, Davies MJ, Born GV (1989) Influence of plaque configuration and stress distribution on fissuring of coronary atherosclerotic plaques. *Lancet* 2(8669):941–944.
10. Maldonado N, et al. (2012) A mechanistic analysis of the role of microcalcifications in atherosclerotic plaque stability: Potential implications for plaque rupture. *Am J Physiol Heart Circ Physiol* 303(5):H619–H628.
11. Virmani R, Burke AP, Kolodgie FD, Farb A (2003) Pathology of the thin-cap fibroatheroma: A type of vulnerable plaque. *J Interv Cardiol* 16(3):267–272.
12. Cheng GC, Loree HM, Kamm RD, Fishbein MC, Lee RT (1993) Distribution of circumferential stress in ruptured and stable atherosclerotic lesions. A structural analysis with histopathological correlation. *Circulation* 87(4):1179–1187.
13. Bobryshev YV, Killingsworth MC, Lord RS, Grabs AJ (2008) Matrix vesicles in the fibrous cap of atherosclerotic plaque: Possible contribution to plaque rupture. *J Cell Mol Med* 12(5B):2073–2082.
14. Aikawa E, et al. (2007) Osteogenesis associates with inflammation in early-stage atherosclerosis evaluated by molecular imaging in vivo. *Circulation* 116(24):2841–2850.
15. Hsu HH, Camacho NP (1999) Isolation of calcifiable vesicles from human atherosclerotic aortas. *Atherosclerosis* 143(2):353–362.
16. Aikawa E, et al. (2009) Arterial and aortic valve calcification abolished by elastolytic cathepsin S deficiency in chronic renal disease. *Circulation* 119(13):1785–1794.
17. Maldonado N, Kelly-Arnold A, Cardoso L, Weinbaum S (2013) The explosive growth of small voids in vulnerable cap rupture; cavitation and interfacial debonding. *J Biomech* 46(2):396–401.
18. Gent AN, Park B (1984) Failure processes in elastomers at or near a rigid spherical inclusion. *J Mater Sci* 19(6):1947–1956.
19. Virmani R, et al. (2007) The pathology of vulnerable plaque. *The Vulnerable Atherosclerotic Plaque: Strategies for Diagnosis and Management*, eds Virmani R, Narula J, Leon M, Willerson JTE (Blackwell, Malden, MA), pp 21–36.
20. Ohayon J, et al. (2008) Necrotic core thickness and positive arterial remodeling index: Emergent biomechanical factors for evaluating the risk of plaque rupture. *Am J Physiol Heart Circ Physiol* 295(2):H717–H727.
21. Akyildiz AC, et al. (2011) Effects of intima stiffness and plaque morphology on peak cap stress. *Biomed Eng Online* 10:25.
22. New SE, Aikawa E (2011) Cardiovascular calcification: An inflammatory disease. *Circ J* 75(6):1305–1313.
23. Roijers RB, et al. (2011) Microcalcifications in early intimal lesions of atherosclerotic human coronary arteries. *Am J Pathol* 178(6):2879–2887.
24. Shanahan CM, Crouthamel MH, Kapustin A, Giachelli CM (2011) Arterial calcification in chronic kidney disease: Key roles for calcium and phosphate. *Circ Res* 109(6):697–711.
25. Wenk JF, Papadopoulos P, Zohdi TI (2010) Numerical modeling of stress in stenotic arteries with microcalcifications: A micromechanical approximation. *J Biomech Eng* 132(9):091011.
26. Ohayon J, et al. (2007) Influence of residual stress/strain on the biomechanical stability of vulnerable coronary plaques: Potential impact for evaluating the risk of plaque rupture. *Am J Physiol Heart Circ Physiol* 293(3):H1987–H1996.